

Appearance Reconstruction of Fluorescent Objects Based on Reference Geometric Factors

Shoji Tominaga; Norwegian University of Science and Technology, Gjøvik, Norway / Nagano University, Ueda, Japan
Keita Hirai, Takahiko Horiuchi; Department of Imaging Sciences, Chiba University, Chiba, Japan.

Abstract

An approach is proposed for the reliable appearance reconstruction of fluorescent objects under arbitrary conditions of material and illuminant based on reference geometric factors. First, a large set of spectral images is acquired from a variety of scenes of fluorescent objects paired with a mutual illumination effect under different conditions. The target fluorescent object is constructed using a cube and a flat plate supporting it, and is subsequently illuminated using a directional light source. We produce many target objects of the same size with different fluorescent materials and observe them under different illumination conditions. The observed spectral images are subsequently decomposed into five components, combining the spectral functions and geometric factors. The reference geometric factors are independent of the material, illuminant, and illumination direction change; instead, they are only dependent on object geometries. A reliable estimation method of reference geometric factors is presented using the whole spectral images observed under various conditions. Further, we propose an algorithm for reconstructing a realistic appearance including mutual illumination effect under arbitrary conditions of material, illuminant, and illumination direction. Finally, the reliability of the proposed approach is examined experimentally.

Introduction

Fluorescent spectral characteristics are described in terms of the bispectral radiance factor that is a function of two wavelength variables: the excitation wavelength of the incident light and the emission/reflection wavelength. The bispectral radiance factor can be summarized as a Donaldson matrix [1], which is an illuminant-independent matrix representation of the bispectral characteristics of a target object [2]. Therefore, once we determine the Donaldson matrix, the appearance of the object observed under arbitrary illumination can be reconstructed spectrally using the illuminant spectral-power distribution of the light source.

A reconstruction of the appearance of objects with different material properties, or from different illumination directions or under different illuminant spectra, is often necessary in daily life. The creation of plausible novel object appearances under different conditions is occasionally called appearance control or appearance editing [3]. The overall appearance of three-dimensional (3D) objects in a scene is resulted from a combination of chromatic factors, such as the reflectance, luminescence spectra, and scene illuminant, as well as geometric factors such as the surface geometry, texture, and lighting conditions. In addition, real scenes often exhibit a significant mutual illumination between their surfaces. Because the mutual illumination is accompanied with a change in the appearance of the object surfaces, its influence must be considered in appearance reconstruction [4, 5]. The effects of

mutual illumination depend on the surface materials and geometries.

A previous study [6, 7] presented a method for the appearance reconstruction of fluorescent objects under different spectral characteristics of material and illuminant. The scene appearance including two fluorescent objects was decomposed into several components, each of which was described by spectral functions and geometric factors. It was demonstrated that the scene appearance of the target objects with different material characteristics under different illuminants could be reconstructed by replacing the terms of spectral functions with the target spectra. Further, the reference geometric factors were defined to estimate the geometric factors of object surfaces at general observation conditions. However, the reference geometric factors were estimated under the limited conditions of fluorescent material and illuminant.

The present paper aims to develop a reliable appearance reconstruction of fluorescent objects under arbitrary conditions of material and illuminant based on the reference geometric factors. Hence, we first generate a large set of spectral images acquired from a variety of scenes of two fluorescent objects with a mutual illumination effect under different conditions. The target scene is a cubic fluorescent object placed on a flat fluorescent plane, which are illuminated by a directional light source. Such an object with the same size is produced with different fluorescent materials and observed under different illumination directions and different illuminant spectra. The observed images of the same fluorescent materials are subsequently decomposed into several components based on spectral compositions. Each component image is represented by combining the spectral functions and geometric factors. The geometric factors are spectrally independent and changed for different illumination directions.

Next, the reference geometric factors are independent of material, illuminant, and illumination direction change; instead, they are only dependent on object geometries. We determine the reference geometric factors based on the whole set of observed spectral images under various conditions. In this process, image registration is used to align the spectral images captured for different fluorescent objects. We present an algorithm for reconstructing a realistic appearance including the mutual illumination effect under arbitrary conditions of material, illuminant, and illumination direction. Finally, experiments are conducted to demonstrate the reliability of the proposed method. The accuracy is evaluated in detail.

Image Formation with Mutual Illumination

The bispectral radiance factor of a fluorescent object is a function of the excitation wavelength λ_{em} and emission/reflection wavelength λ_{ex} (see [1]). In this study, the excitation range is set to $350 \leq \lambda_{ex} \leq 700$ (nm); because our spectral imaging system operates in the visible range, the emission/reflection range is set as $400 \leq \lambda_{em} \leq 700$ (nm). Let

$S(\lambda)$, $\alpha(\lambda_{em})$, and $\beta(\lambda_{ex})$ be the surface-spectral reflectance at $\lambda_{em} = \lambda_{ex}$, the emission spectrum, and the excitation spectrum, respectively. We assume $\int_{350}^{700} \beta(\lambda_{ex}) d\lambda_{ex} = 1$ (see [2]).

When we observe a matte surface of a fluorescent material under a single illuminant $E(\lambda)$, the spectral radiance observed at location $\mathbf{x} = (x, y)$ of the object surface can be described as

$$y(\mathbf{x}, \lambda_{em}) = f_{ref}(\mathbf{x})S(\lambda_{em})E(\lambda_{em}) + f_{lum}(\mathbf{x})\alpha(\lambda_{em})\int_{350}^{\lambda_{em}} \beta(\lambda_{ex})E(\lambda_{ex})d\lambda_{ex} \quad (1)$$

where the first and second terms in the right side represent the reflection radiance and luminescence radiance, respectively. The weights $f_{ref}(\mathbf{x})$ and $f_{lum}(\mathbf{x})$ for the spectral functions represent the geometric factors, depending on the object surface geometry and location.

Suppose that flat objects with different bispectral characteristics are located closely, as shown in Figure 1. Assuming that the mutual illumination is based only on one bounce of the light ray between the two surfaces, the observations from surface i can be represented as

$$y_i(\mathbf{x}, \lambda_{em}) = f_{i1}(\mathbf{x})S_i(\lambda_{em})E(\lambda_{em}) + f_{i2}(\mathbf{x})S_i(\lambda_{em})S_j(\lambda_{em})E(\lambda_{em}) + f_{i3}(\mathbf{x})C_{i1}(\lambda_{em})\alpha_i(\lambda_{em}) + f_{i4}(\mathbf{x})C_{i2}(\lambda_{em})\alpha_i(\lambda_{em}) + f_{i5}(\mathbf{x})C_{i3}(\lambda_{em})\alpha_i(\lambda_{em}) + f_{i6}(\mathbf{x})C_{i4}(\lambda_{em})S_i(\lambda_{em})\alpha_j(\lambda_{em}) \quad (2)$$

where $(i=1, j=2)$ or $(i=2, j=1)$, and

$$\begin{aligned} C_{i1}(\lambda_{em}) &= \int_{350}^{\lambda_{em}} \beta_i(\lambda_{ex})E(\lambda_{ex})d\lambda_{ex}, \\ C_{i2}(\lambda_{em}) &= \int_{350}^{\lambda_{em}} \beta_i(\lambda_{ex})S_j(\lambda_{ex})E(\lambda_{ex})d\lambda_{ex}, \\ C_{i3}(\lambda_{em}) &= \int_{350}^{\lambda_{em}} \beta_i(\lambda_{ex})\alpha_j(\lambda_{ex})\left[\int_{350}^{\lambda_{ex}} \beta_j(\lambda'_{ex})E(\lambda'_{ex})d\lambda'_{ex}\right]d\lambda_{ex}, \\ C_{i4}(\lambda_{em}) &= \int_{350}^{\lambda_{em}} \beta_j(\lambda_{ex})E(\lambda_{ex})d\lambda_{ex}. \end{aligned} \quad (3)$$

Equation (2) suggests that the spectral radiance observed from each surface is described in a linear combination of six types of spectral functions. The respective compositions represent (1) diffuse reflection on the matte surface, (2) diffuse-diffuse interreflection, (3) luminescence based on direct illumination, (4) luminescence caused by reflected light from another surface, (5) luminescence caused by fluorescent illumination from another surface, and (6) interreflection caused by fluorescent illumination from another surface. The spectral functions $C_{i1}(\lambda_{em})$, $C_{i2}(\lambda_{em})$, and $C_{i3}(\lambda_{em})$ are constant in longer wavelength with $\beta_i(\lambda) = 0$, and the emission function $\alpha_i(\lambda)$ is small in lower wavelength. Consequently, $C_{i1}(\lambda_{em})\alpha_i(\lambda_{em})$, $C_{i2}(\lambda_{em})\alpha_i(\lambda_{em})$, and $C_{i3}(\lambda_{em})\alpha_i(\lambda_{em})$ are of the same shape as $\alpha_i(\lambda_{em})$, spectrally.

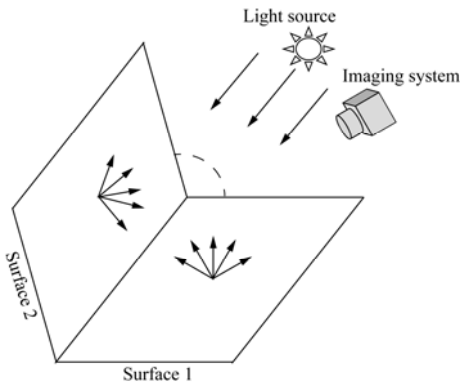


Figure 1. Observations of two flat matte surfaces with different bispectral characteristics under a directional illumination.

Appearance Decomposition

Because the three luminescence components cannot be decomposed spectrally, we conducted the appearance decomposition in two steps. In the first step, we unify the luminescence functions as $\alpha_i(\lambda_{em})$, and decomposed the observed image based on four spectral functions with an independent spectral shape. In the second step, the obtained luminescence component is further decomposed based on the spatial distribution.

Let $\mathbf{s}_i (i=1,2)$ and $\mathbf{a}_i (i=1,2)$ be N-dimensional column vectors representing the reflectance and emission spectra of surface i . In addition, let $\mathbf{c}_{ij} (i=1,2, j=1,2,\dots,4)$ be N-dimensional column vectors representing the spectral functions $C_{ij}(\lambda) (i=1,2, j=1,2,\dots,4)$. The observations are then modeled in a simple matrix equation as (see [6])

$$\mathbf{y}_1(\mathbf{x}) = \mathbf{A}_1 \mathbf{f}_1(\mathbf{x}), \quad \mathbf{y}_2(\mathbf{x}) = \mathbf{A}_2 \mathbf{f}_2(\mathbf{x}), \quad (4)$$

where the matrices of spectral component functions are given as

$$\begin{aligned} \mathbf{A}_1 &= [\mathbf{s}_1 \cdot \mathbf{e} \quad \mathbf{s}_1 \cdot \mathbf{s}_2 \cdot \mathbf{e} \quad \mathbf{c}_{11} \cdot \mathbf{a}_1 \quad \mathbf{c}_{12} \cdot \mathbf{s}_1 \cdot \mathbf{a}_2], \\ \mathbf{A}_2 &= [\mathbf{s}_2 \cdot \mathbf{e} \quad \mathbf{s}_1 \cdot \mathbf{s}_2 \cdot \mathbf{e} \quad \mathbf{c}_{21} \cdot \mathbf{a}_2 \quad \mathbf{c}_{22} \cdot \mathbf{s}_2 \cdot \mathbf{a}_1] \end{aligned} \quad (5)$$

and the geometric factors at location \mathbf{x} as follows:

$$\begin{aligned} \mathbf{f}_1(\mathbf{x}) &= [f_{11}(\mathbf{x}) \quad f_{12}(\mathbf{x}) \quad f_{13}(\mathbf{x}) \quad f_{14}(\mathbf{x})]^t, \\ \mathbf{f}_2(\mathbf{x}) &= [f_{21}(\mathbf{x}) \quad f_{22}(\mathbf{x}) \quad f_{23}(\mathbf{x}) \quad f_{24}(\mathbf{x})]^t \end{aligned} \quad (6)$$

Because $\mathbf{A}_i^t \mathbf{A}_i (i=1,2)$ are of full rank, and the estimates of $\mathbf{f}_i(\mathbf{x}) (i=1,2)$ are determined at every location \mathbf{x} using the standard linear least-squares method; thus, the observed spectral radiance image is decomposed into four spectral component images.

Next, recall that the luminescence component above is composed of three types of optical processes. One type is the emissions excited by direct illumination from a light source, and the other two types are emissions excited by the reflection and emission of light from another surface. We assume that the fluorescence emission is Lambertian, that is, the ideal diffuse radiation. Therefore, the similarity between the reflection on a Lambertian surface and the fluorescence emission results in two types of fluorescent emissions by direct and indirect illuminations corresponding to the two reflection types of the diffuse reflection by direct illumination and diffuse-diffuse interreflection. The geometric factors for reflection and inter-reflection are different in a spatial distribution within the entire area including the two objects. Thus, the luminescence geometric factor $f_3(\mathbf{x}) = \{f_{13}(\mathbf{x}), f_{23}(\mathbf{x})\}$ is further decomposed into direct and indirect illumination components as $f_3(\mathbf{x}) = w_1 f_1(\mathbf{x}) + w_2 f_2(\mathbf{x})$, where $f_1(\mathbf{x}) = \{f_{11}(\mathbf{x}), f_{21}(\mathbf{x})\}$ and $f_2(\mathbf{x}) = \{f_{12}(\mathbf{x}), f_{22}(\mathbf{x})\}$ are the geometric factors of the diffuse reflection and diffuse-diffuse interreflection in Eq. (6). The scalar weights w_1 and w_2 are estimated over the entire area using the standard linear least-squares method to minimize the residual error $\|f_3(\mathbf{x}) - \hat{f}_3(\mathbf{x})\|^2$ using the estimated \hat{f} . Finally, the observed spectral images are decomposed into five physical components of (1) diffuse reflection, (2) diffuse-diffuse interreflection, (3) luminescence excited by direct illumination, (4) luminescence excited by indirect illumination, and (5) interreflection caused by fluorescent illumination.

Estimation of Reference Geometric Factors

Modeling

All geometric factors $f_1(\mathbf{x}) - f_5(\mathbf{x})$ are dependent on the illumination direction. The reference geometric factors are defined as the invariant representations of the geometric factors, independent of directional change in illumination. We determine the reference geometric factors by considering the models of reflectance, luminescence, and mutual illumination for two Lambertian matte surfaces, as shown in Figure 2, where \mathbf{n}_1 and \mathbf{n}_2 are the surface normal vectors, and \mathbf{l} is the illumination directional vector. When we adopt Hurlber's model [8], the spectral radiance observed by a diffuse reflection is described as

$$\begin{aligned} y_{11}(\mathbf{x}, \lambda) &= f_{o1}(\mathbf{x})(\mathbf{n}_1 \cdot \mathbf{l}) S_1(\lambda) E(\lambda), & \text{for Surface 1} \\ y_{12}(\mathbf{x}, \lambda) &= f_{o1}(\mathbf{x})(\mathbf{n}_2 \cdot \mathbf{l}) S_2(\lambda) E(\lambda), & \text{for Surface 2} \end{aligned} \quad (7)$$

where $f_{o1}(\mathbf{x})$ is defined as the geometric factor in the case of vertical incidence to each surface. This factor can be constant, independently of \mathbf{x} for an ideal flat surface.

$$\begin{aligned} y_{21}(\mathbf{x}, \lambda) &= f_{o2}(\mathbf{x})(\mathbf{n}_2 \cdot \mathbf{l}) S_1(\lambda) S_2(\lambda) E(\lambda), & \text{for Surface 1} \\ y_{22}(\mathbf{x}, \lambda) &= f_{o2}(\mathbf{x})(\mathbf{n}_1 \cdot \mathbf{l}) S_1(\lambda) S_2(\lambda) E(\lambda), & \text{for Surface 2} \end{aligned} \quad (8)$$

where $f_{o2}(\mathbf{x})$ represents the reference geometric factor for the case of incidence from the direction bisecting two plane surfaces (see Figure 2). When the illumination is parallel to the bisection of the two planes, each surface receives the same amount of light.

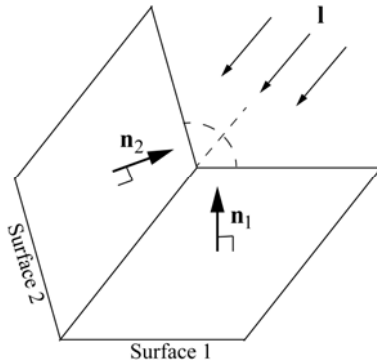


Figure 2. Directional vector bisecting the two adjacent plane surfaces.

Basic estimation algorithm

The surface normal vectors \mathbf{n}_1 and \mathbf{n}_2 at each location of the object surface were estimated using a photometric stereo method [6] that was based on changes in shading under different illumination directions. Because the illumination directional vector \mathbf{l} is known in advance, the reference geometric factors $f_{o1}(\mathbf{x})$ and $f_{o2}(\mathbf{x})$ can be estimated through a comparison of Eqs. (7) and (8) with Eq. (6). The factors $f_{o1}(\mathbf{x})$ for a diffuse reflection are calculated from the observed geometric factors $f_i(\mathbf{x})$ as

$$\begin{aligned} f_{o1}(\mathbf{x}) &= f_1(\mathbf{x}) / (\mathbf{n}_1 \cdot \mathbf{l}), & \text{for Surface 1} \\ f_{o1}(\mathbf{x}) &= f_1(\mathbf{x}) / (\mathbf{n}_2 \cdot \mathbf{l}). & \text{for Surface 2} \end{aligned} \quad (9)$$

Because the directional vector bisecting the two planes is $\mathbf{n} = (\mathbf{n}_1 + \mathbf{n}_2) / \sqrt{2 \cdot \sqrt{1 + \mathbf{n}_1 \cdot \mathbf{n}_2}}$, $f_{o2}(\mathbf{x})$ for interreflection are calculated as

$$\begin{aligned} f_{o2}(\mathbf{x}) &= f_2(\mathbf{x}) \sqrt{1 + \mathbf{n}_1 \cdot \mathbf{n}_2} / (\sqrt{2} \mathbf{n}_2 \cdot \mathbf{l}), & \text{for Surface 1} \\ f_{o2}(\mathbf{x}) &= f_2(\mathbf{x}) \sqrt{1 + \mathbf{n}_1 \cdot \mathbf{n}_2} / (\sqrt{2} \mathbf{n}_1 \cdot \mathbf{l}), & \text{for Surface 2} \end{aligned} \quad (10)$$

Because the luminescence radiance factor exhibits the same property as the reflection radiance factor, the reference geometric factors $f_{o3}(\mathbf{x})$ are estimated as follows:

$$\begin{aligned} f_{o3}(\mathbf{x}) &= f_3(\mathbf{x}) / (\mathbf{n}_1 \cdot \mathbf{l}), & \text{for Surface 1} \\ f_{o3}(\mathbf{x}) &= f_3(\mathbf{x}) / (\mathbf{n}_2 \cdot \mathbf{l}), & \text{for Surface 2} \end{aligned} \quad (11)$$

The factors $f_{o4}(\mathbf{x})$ and $f_{o5}(\mathbf{x})$ can be estimated similarly as the interreflection:

$$\begin{aligned} f_{oi}(\mathbf{x}) &= f_i(\mathbf{x}) \sqrt{1 + \mathbf{n}_1 \cdot \mathbf{n}_2} / (\sqrt{2} \mathbf{n}_2 \cdot \mathbf{l}), & \text{for Surface 1} \\ f_{oi}(\mathbf{x}) &= f_i(\mathbf{x}) \sqrt{1 + \mathbf{n}_1 \cdot \mathbf{n}_2} / (\sqrt{2} \mathbf{n}_1 \cdot \mathbf{l}), & \text{for Surface 2} \end{aligned} \quad (12)$$

where $i = 4, 5$.

Global estimation based on multiple observations

To improve the reliability of the factor estimation, the reference geometric factors are estimated not based on a single set but on the whole set of observed spectral images under various conditions. However, it is noteworthy that the captured images for different sets of fluorescent objects contain registration errors. Figure 3 demonstrates an example of registration errors occurring when overlaying two captured images. The errors appear to be caused by rotation and shift. Subsequently, an image registration technique is adopted to align the spectral images captured for different fluorescent objects. First, we produce a mask image for the image capture, as shown in Figure 4, where the mask image represents segmentation into four flat surfaces. Next, affine transformation is applied to correct the registration errors between the two mask images. Let \mathbf{T} be the affine transformation matrix. This matrix is applied to the reference geometric factors as $\mathbf{T}f_{oi}(\mathbf{x})$ ($i=1, 2, \dots, 5$). Finally, the whole set of corrected reference geometric factors are averaged for each of the five components.

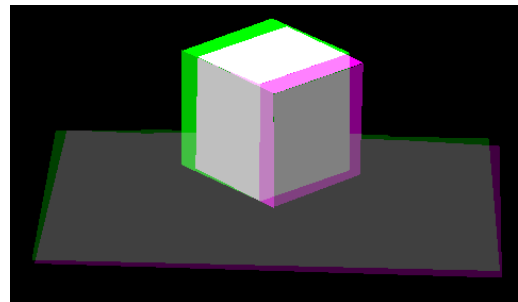


Figure 3. Registration errors when overlaying two captured images.

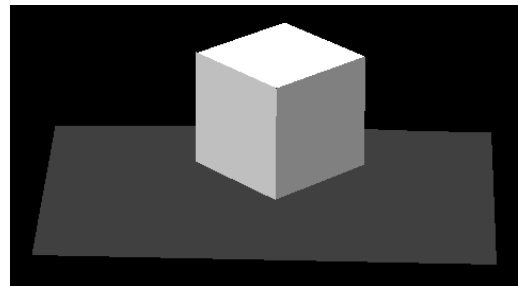


Figure 4. Mask image representing segmentation into four flat surfaces.

Appearance Reconstruction

We construct a new appearance for a pair of fluorescent objects under different fluorescent materials, illuminant spectra, and illuminant direction conditions using the estimated reference geometric factors. The new spectral images were produced at the respective levels of the five components. First, we predicted the geometric factors $f_1(\mathbf{x}), f_2(\mathbf{x}), f_3(\mathbf{x}), f_4(\mathbf{x}), f_5(\mathbf{x})$ for a new direction \mathbf{l}' of the light source. This prediction algorithm resulted in the reversal process used to derive the reference geometric factor $f_{o1}(\mathbf{x}), f_{o2}(\mathbf{x}), f_{o3}(\mathbf{x}), f_{o4}(\mathbf{x}), f_{o5}(\mathbf{x})$ from the observed geometric factors. In practice, the geometric factors for direction \mathbf{l}' are predicted as follows:

$$f'_{ij}(\mathbf{x}) = (\mathbf{n}_j \cdot \mathbf{l}') f_{oi}(\mathbf{x}), \quad (i=1,3) \quad (j=1,2) \quad (13)$$

$$f'_{ij}(\mathbf{x}) = ((\sqrt{2}\mathbf{n}_j \cdot \mathbf{l}') / \sqrt{1+\mathbf{n}_1 \cdot \mathbf{n}_2}) f_{oi}(\mathbf{x}), \quad (i=2,4,5) \quad (j=1,2)$$

where i and j represent the component and surface number.

Next, we can extract the fluorescent materials and illuminant spectrum from their databases. The total bispectral characteristics of the two desired fluorescent materials are specified by a pair of spectral functions $(S_j(\lambda), \alpha_j(\lambda), \beta_j(\lambda))$ ($j=1,2$) constituting the Donaldson matrices. The spectral functions for the five components are summarized as follows:

$$\mathbf{A}'_1 = [s_1 \cdot \mathbf{e} \quad s_1 \cdot s_2 \cdot \mathbf{e} \quad \mathbf{c}'_{11} \cdot \mathbf{a}_1 \quad \mathbf{c}'_{11} \cdot \mathbf{a}_1 \quad \mathbf{c}'_{12} \cdot s_1 \cdot \mathbf{a}_2],$$

$$\mathbf{A}'_2 = [s_2 \cdot \mathbf{e} \quad s_1 \cdot s_2 \cdot \mathbf{e} \quad \mathbf{c}'_{21} \cdot \mathbf{a}_2 \quad \mathbf{c}'_{21} \cdot \mathbf{a}_2 \quad \mathbf{c}'_{22} \cdot s_2 \cdot \mathbf{a}_2], \quad (14)$$

where \mathbf{c}'_{i1} and \mathbf{c}'_{i2} ($i=1,2$) associated with the spectral functions of the new materials are determined using $\mathbf{c}'_{i1}=1$ and $\mathbf{c}'_{i2}=\mathbf{c}'_{i4}$ in Eq. (4).

The component spectral images at the respective levels are rendered by combining the spectral functions and geometric factors as $f_{i1}(\mathbf{x}) \times \mathbf{S}'_{1i}$ and $f_{i2}(\mathbf{x}) \times \mathbf{S}'_{2i}$ ($i=1,2,\dots,5$). The spectral radiances of the new scene appearance under the desired material and illumination conditions are reconstructed using a linear sum of the five components at every location as

$$\mathbf{y}'_1(\mathbf{x}) = \mathbf{A}'_1 \mathbf{f}'_1(\mathbf{x}), \quad \mathbf{y}'_2(\mathbf{x}) = \mathbf{A}'_2 \mathbf{f}'_2(\mathbf{x}), \quad (15)$$

where $\mathbf{f}'_j = [f'_{1j} \quad f'_{2j} \quad f'_{3j} \quad f'_{4j} \quad f'_{5j}]^T$ ($j=1,2$). The N -dimensional radiance vectors above are finally converted into a display color space where a color image of the reconstructed appearance is rendered within the visible range.

Experiments

Image acquisition

Our spectral imaging system consisted of a monochrome CCD camera with a 12-bit dynamic range and Peltier cooling, a VariSpec liquid crystal tunable filter, an IR cut filter, and a personal computer. The spectral images of the fluorescent objects were captured at 5-nm intervals within the visible wavelength range of 400 to 700 nm; thus, each captured image was represented in an array of 61 (=N)-dimensional vectors. We used three light sources: (1) an incandescent lamp (Iwasaki, PRF-300W), (2) a flood daylight lamp used for photography (Iwasaki, PRF-350WD), and (3) an artificial sunlight (Seric, SOLAX 100 W). Figure 5 shows the illuminant spectral-power distributions of three light sources. A white reference board was placed at the same position as the target objects to standardize the captured images and eliminate nonuniformity in the illumination.

The target object was constructed using a cube and a flat plate supporting it, the surfaces of which were composed of green, pink, red, and yellow fluorescent sheets (Lumino Sheet, Okina Inc.). Thus, we selected two combinations of (1) (green, pink) and (2) (red, yellow) from the four different fluorescent materials. Figures 6–7 show the spectral functions $S(\lambda)$, $\alpha(\lambda_{em})$, and $\beta(\lambda_{ex})$ for the four fluorescent materials, which were obtained using the method in Ref. 9. Each target object was illuminated from the five directions of (1) extreme upper, (2) upper left, (3) upper right, (4) middle upper, and (5) front. Figure 8 shows a color image set of the whole spectral images captured under the different conditions of the four fluorescent materials, three illuminants, and five illumination directions.

Results of estimation and reconstruction

Figure 9 shows a set of reference geometric factors estimated using the whole spectral images in Figure 8, where the images represent the spatial distributions of the five reference geometric factors. Image rendering for the appearance reconstruction was conducted based on the reference geometric factors and assumed fluorescent material, illuminant, and illumination direction.

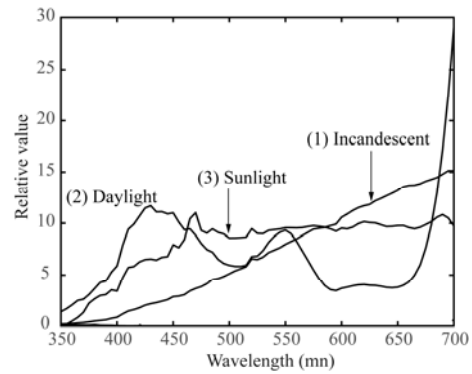


Figure 5. Illuminant spectral-power distributions of three light sources.

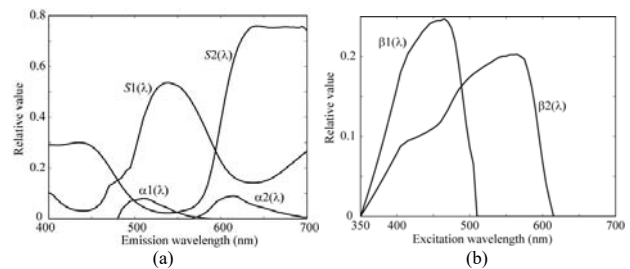


Figure 6. Spectral functions of green and pink fluorescent materials: (a) reflectance and emission functions, and (b) excitation functions.

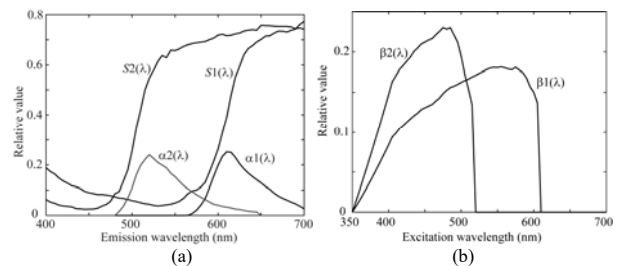


Figure 7. Spectral functions of red and yellow fluorescent materials: (a) reflectance and emission functions, and (b) excitation functions.

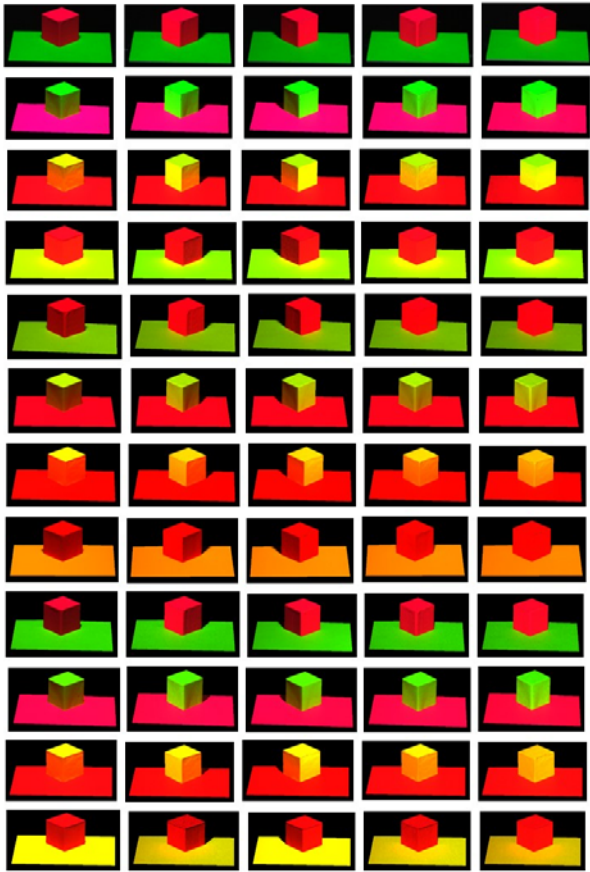


Figure 8. Color image set of the whole spectral images captured under different conditions.

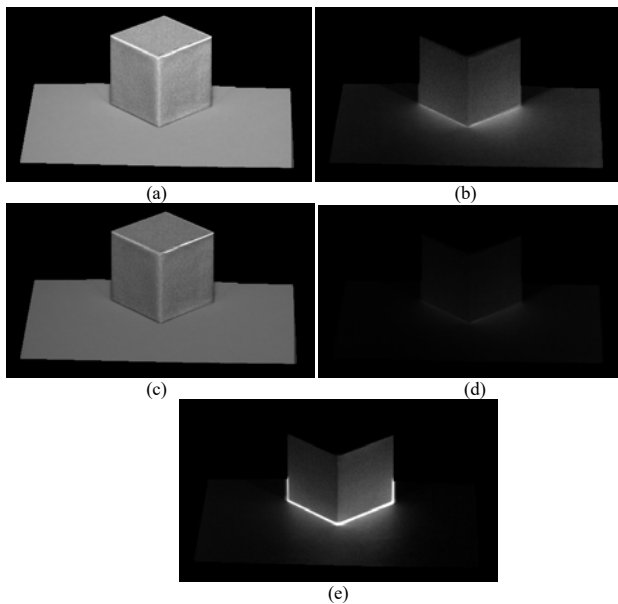


Figure 9. Set of the estimated reference geometric factors: (a) $f_{o1}(\mathbf{x})$, (b) $f_{o2}(\mathbf{x})$, (c) $f_{o3}(\mathbf{x})$, (d) $f_{o4}(\mathbf{x})$, and (e) $f_{o5}(\mathbf{x})$.

Figure 10 shows the reconstruction results for a yellow cube and a red flat plate supporting it, where the objects were supposed to be illuminated using the daylight lamp from the upper left. In the figure, (a)–(e) show the component images produced during the reconstruction process, and (f) shows the

color image of the reconstruction result using the linear sum of the five component images. The cube casts a shadow on the plate through a direct tilted illumination. The shadow cast was additionally rendered by the known illuminant direction and object size.

Evaluation

The accuracy of the proposed method for the appearance reconstruction of fluorescent objects was evaluated both visually and numerically. All captured images and reconstructed results are displayed in the sRGB color space to reproduce the color appearance in a calibrated display device. Hence, all spectral images were first transformed into CIE-XYZ images using the color-matching functions, and subsequently converted into sRGB images. An appearance comparison was conducted visually on a calibrated monitor between the reconstructed images and captured images of real objects, as shown in Figure 8. For instance, the real image for Figure 10 (f) corresponds to the image in the (3, 2) element of Figure 8. Figure 11 shows the difference image of luminance Y between the reconstructed and real images.

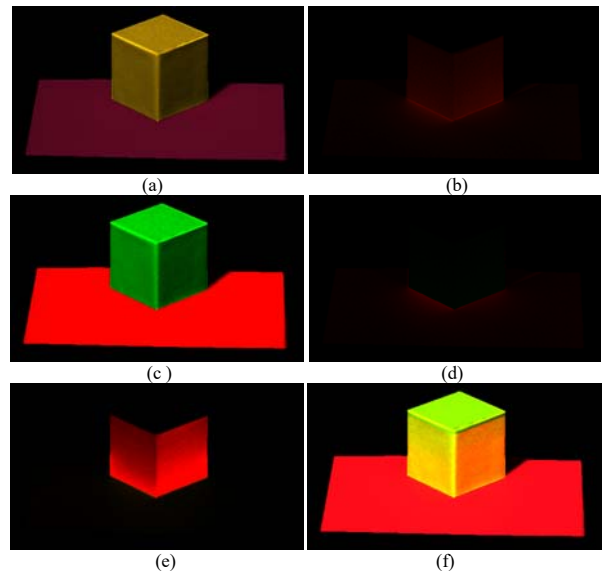


Figure 10. Reconstruction results for a yellow cube and a red flat plate supporting it, where the objects were supposed to be illuminated using the daylight lamp from the upper left. (a)–(e): Component images of diffuse reflection, interreflection, luminescence by direct illumination, luminescence by indirect illumination, interreflection by fluorescent illumination. (f): Scene reconstructed using a linear sum of the component images.

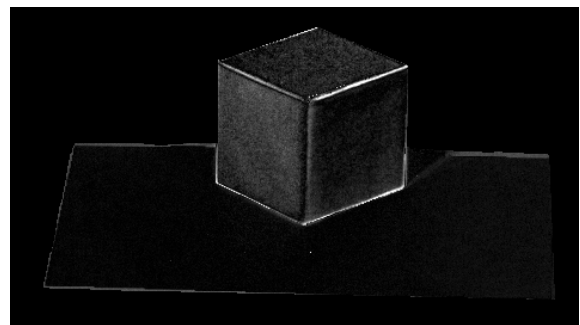


Figure 11. Difference image of luminance Y between the reconstructed and real images.

Table 1. Average color differences over five illumination directions in the case of a yellow cube and a red flat plate.

	XYZ difference	sRGB difference
Average reconstruction error	0.1667	0.1027
1. Reflection	0.0721	0.0954
2. Interreflection	0.0110	0.0218
3. Luminescence by direct	0.1041	0.1914
4. Luminescence by indirect	0.0100	0.0205
5. Interreflection by fluorescence	0.0365	0.0554

To quantify the reconstruction error numerically, the color differences are calculated between the reconstructed image and real object image. A registration error occurs between the captured image of a real object scene and the reconstructed image. The registration error was corrected using the affine transformation similarly as in estimation of the reference geometric factors. It is noteworthy that the LAB color space defined on object color is not available for fluorescent colors. Therefore, we calculated the color differences in the XYZ and sRGB spaces. Table 1 demonstrates the average color differences over five illumination directions in the case of a yellow cube and a red flat plate. The real object images correspond to the third row in Figure 7. In Table 1, the tristimulus values XYZ and the sRGB values are normalized such that the average luminance value Y is 0.5 and $0 \leq R, G, B \leq 1$. We decomposed the total reconstruction error into five components based on the spectral functions. Large error appeared in the luminescence component from direct illumination. This is because the luminescence color by fluorescence emission is highly chromatic and saturated, and the color coordinates are located outside of the sRGB gamut.

Conclusions

We herein proposed an approach for the reliable appearance reconstruction of fluorescent objects under arbitrary conditions of material and illuminant based on the reference geometric factors. First, we created a large set of spectral images acquired from a variety of scenes of fluorescent objects paired with a mutual illumination effect under different conditions. The target object was constructed using a cube and a flat plate supporting it, which were illuminated using a directional light source. Such objects of the same size were produced with different fluorescent materials and observed under different illumination conditions. The observed spectral images were subsequently decomposed into five components, each of which was represented by combining the spectral functions and geometric factors. Second, the reference geometric factors were independent of the material, illuminant, and illumination direction change; instead, they were only dependent on object geometries. We estimated the reference geometric factors from the whole spectral images observed

under various conditions. Finally, the reliability of the proposed approach was examined experimentally, and the accuracy of the appearance reconstruction was evaluated numerically.

In this paper, we assumed that fluorescent objects have plane surfaces. The extension to more general object shapes remains for future study.

Acknowledgements

This work was supported by Research Council of Norway (MUVApp project, 250293), and Japan Society for the Promotion of Science (JSPS) (15H05926).

References

- [1] R. Donaldson, "Spectrophotometry of fluorescent pigments," *British J. of Applied Physics*, vol. 5, no. 6, pp. 210–214, 1954.
- [2] S. Tominaga, K. Hirai, and T. Horiuchi, "Estimation of bispectral Donaldson matrices of fluorescent objects by using two illuminant projections," *J. Optical Society of America A*, vol. 32, no. 6, pp. 1068–1078, 2015.
- [3] A. Serrano, K. Myszkowski, H.P. Seidel, and B. Masia, "An intuitive control space for material appearance," *ACM Trans. Graphics*, vol. 35, issue 6, article no. 186, 2016.
- [4] R. Carroll, R. Ramamoorthi, and M. Agrawala, "Illumination decomposition for material recoloring with consistent interreflections," *ACM Trans. Graphics*, vol. 30, no. 4, article no. 43, 2011.
- [5] S. Tominaga, K. Kato, K. Hirai, and T. Horiuchi, "Appearance reconstruction of fluorescent objects for different materials and light source," *Proc. 25th Color and Imaging Conf.*, pp. 34–39, 2017.
- [6] S. Tominaga, K. Kato, K. Hirai, and T. Horiuchi, "Appearance reconstruction of 3D fluorescent objects under different conditions," *Proc. 26th Color and Imaging Conf.*, pp. 44–48, 2018.
- [7] S. Tominaga, K. Hirai, and T. Horiuchi, "Appearance reconstruction of mutual illumination effect between plane and curved fluorescent objects," *Proc. IS&T Inter. Sympo. on Electronic Imaging, Material Appearance 2019*, pp. 485-1 - 485-5, 2019.
- [8] A. C. Hurlbert, "Computational models of color constancy," in: V. Walsh and J. Kulikowski (Eds), *Perceptual Constancy: Why things look as they do*, pp. 283–321, Cambridge University Press, 1998.
- [9] S. Tominaga, K. Hirai, and T. Horiuchi, "Estimation of fluorescent Donaldson matrices using a spectral imaging system," *Optics Express*, vol. 26, no. 2, pp. 2132–2148, 2018.

Author Biography

Shoji Tominaga received the B.E., M.S., and Ph.D. degrees in electrical engineering from Osaka University, Japan, in 1970, 1972, and 1975, respectively. He was a Professor (2006–2013) and Dean (2011–2013) at Graduate School in Chiba University. He is now a Professor, Norwegian University of Science and Technology and also a Visiting Researcher, Nagano University. His research interests include digital color imaging, multispectral imaging, and material appearance. He is a Fellow of IEEE, IS&T, SPIE, and OSA.